High-pressure structural and lattice dynamical study of HgWO$_4$

F. J. Manjón,[1,*] J. López-Solano,[2] S. Ray,[1,†] O. Gomis,[3] D. Santamaría-Pérez,[4] M. Mollar,[1] V. Panchal,[5] D. Errandonea,[5]
P. Rodríguez-Hernández,[2] and A. Muñoz[2]

[1]*Instituto de Diseño para la Fabricación y Producción Automatizada, MALTA Consolider Team,
Universitat Politècnica de València, 46022 València, Spain*
[2]*Departamento de Física Fundamental II, MALTA Consolider Team, Universidad de La Laguna, 38205 La Laguna, Tenerife, Spain*
[3]*Centro de Tecnologías Físicas, MALTA Consolider Team, Universitat Politècnica de València, 46022 València, Spain*
[4]*Departamento de Química Física I, MALTA Consolider Team, Universidad Complutense de Madrid,
Avenida Complutense s/n, 28040 Madrid, Spain*
[5]*Instituto de Ciencia de Materiales de la Universitat de València, Fundación General de la Universitat de València,
MALTA Consolider Team, 46100 Burjassot, València, Spain*

We have synthesized monoclinic mercury tungstate (HgWO$_4$) and characterized its structural and vibrational properties at room conditions. Additionally, we report the structural and lattice dynamical behavior of HgWO$_4$ under high pressure studied by means of x-ray diffraction and Raman-scattering measurements up to 16 GPa and 25 GPa, respectively. The pressure dependence of the structural parameters and Raman-active first-order phonons of monoclinic $C2/c$ HgWO$_4$ are discussed in the light of our theoretical first-principles total-energy and lattice dynamics calculations. Our measurements show that the monoclinic phase of HgWO$_4$ is stable up to the maximum pressure reached in these experiments. Theoretically predicted possible high-pressure phases and the theoretical pressure dependence of infrared-active modes are also reported.

PACS number(s): 78.30.−j, 62.50.−p, 63.20.−e

I. INTRODUCTION

Materials belonging to the tungstate family (AWO$_4$) have a long history of practical application, having been first used by Edison in 1896 to detect x rays.[1] Their optical properties, which form the basis of their wide application as phosphors, laser crystals, and scintillation detectors, have made them the object of extensive research.[2–4] New applications for these materials have recently emerged, including large-volume scintillators for high-energy physics[5] and detectors devoted to the search of rare events (e.g., interactions with weakly interactive massive particles).[6] However, mercury tungstate (HgWO$_4$), a wide-band-gap semiconductor with a band-gap energy close to 4 eV (Refs. 7 and 8) and recently proposed as a nanophosphor,[9] is one of the less studied materials of the tungstate family because this compound is difficult to obtain due to the intrinsic instability of Hg compounds.

Depending on the size of the countercation A, AWO$_4$ compounds mostly crystallize at ambient conditions either in the tetragonal scheelite structure [space group (SG): $I4_1/a$, No. 88, $Z=4$], such as CaWO$_4$, SrWO$_4$, BaWO$_4$, and PbWO$_4$, or in the monoclinic wolframite structure (SG: $P2/c$, No. 13, $Z=2$), such as ZnWO$_4$ and CdWO$_4$.[10] In the scheelite structure, W cations have fourfold oxygen coordination while A cations exhibit eightfold oxygen coordination; therefore, the coordination for A and W cations in scheelite, noted as [A cation coordination, W cation coordination], is [8,4]. On the other hand, in the AWO$_4$ wolframite structure W cations have a sixfold (4+2) oxygen coordination while A cations exhibit sixfold oxygen coordination; therefore, cation coordinations in wolframite is noted [6,4+2]. Notable exceptions among tungstates are CuWO$_4$ and HgWO$_4$ which crystallize in structures related to wolframite. CuWO$_4$ crystallizes in a triclinic structure (SG: P-1, No. 2, $Z=2$)

(Ref. 11) while HgWO$_4$ crystallizes in a monoclinic structure (SG: $C2/c$, No. 15, $Z=4$).[12,13] In the latter structure, W cations have a very distorted sixfold (4+2) oxygen coordination while Hg cations exhibit oxygen coordination between 6 and 8 (see Fig. 1). Therefore, from the point of view of A and B cation coordinations in ABO$_4$ compounds, HgWO$_4$ can be seen as an intermediate structure between scheelite and wolframite and its cation coordination can be noted as [6+2, 4+2]. In this sense, HgWO$_4$ is the orthotungstate with the highest total cation coordination (near 14) at room pressure.

High-pressure research has proved to be an efficient tool to improve the understanding of the main physical properties of AWO$_4$ compounds. Although there is abundant literature on high-pressure studies in these materials, much of the research has been carried out on scheelite and wolframite-structured compounds. These studies have been recently
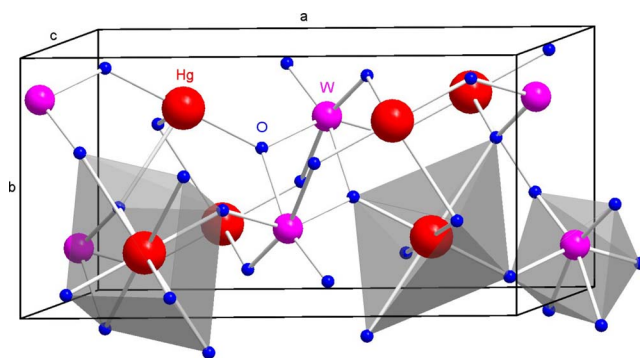

FIG. 1. (Color online) Crystal structure of the monoclinic $C2/c$ structure of HgWO$_4$ at room conditions. The HgO$_6$ octahedra and the more distorted HgO$_8$ dodecahedra are shown for comparison. Note the 180° of the O-Hg-O angle and the large distortion of the WO$_6$ octahedra.

reviewed[14] and it has been established that scheelite tungstates undergo a sequence of pressure-driven structural phase transitions scheelite→M-fergusonite→$BaWO_4$-II. On the contrary, recent high-pressure studies in wolframite tungstates ($MgWO_4$, $ZnWO_4$, and $CdWO_4$) propose a different sequence of pressure-driven structural phase transitions: wolframite→triclinic→β-fergusonite→$Cmca$,[15,16] however, wolframite-type $CdWO_4$ seems to transform to a mixed triclinic and tetragonal scheelite structure prior to the transition to the β-fergusonite phase.[17] The above phase transition sequences for scheelites and wolframites are in good agreement with the conclusions drawn from the application of the crystal chemistry arguments[18] to ABO_4 compounds[15,19] and it remains to be seen if the behavior of $HgWO_4$ follows a similar path like other related AWO_4 compounds and, in particular, those crystallizing in the wolframite structure.

No high-pressure work exists on $HgWO_4$ to the best of our knowledge and even their lattice dynamical properties at room pressure are still poorly known. Only a work reporting some infrared (IR) and Raman frequencies at room pressure is available in the literature.[20] In order to improve the knowledge of the physical properties of AWO_4 compounds under pressure as part of our project to study the structural stability of orthotungstates, we report in this work the complete Raman spectrum at room pressure of $HgWO_4$ and also x-ray diffraction (XRD) and Raman-scattering measurements as a function of pressure. The obtained results are interpreted on the basis of first-principles total-energy and lattice dynamics calculations. The technical aspects of the experiments and calculations are described in Secs. II and III. The results are presented in Sec. IV and discussed in Sec. V. Finally, we present the conclusions of this work in Sec. VI.

II. EXPERIMENTAL DETAILS

$HgWO_4$ powders used in this study were prepared by the solution precipitation method. In a typical synthesis, an equimolar solution of mercury acetate [$Hg(CH_3COO)_2$, Sigma-Aldrich, ACS reagent] and of sodium tungstate (Na_2WO_4, Sigma-Aldrich, ACS reagent) were dissolved in double bidistilled water. In particular, we solved 4 mM of mercury acetate in 50 ml of double distilled water and some drops of $1M$ nitric acid [HNO_3] were added to reach pH=3. To this solution, a new solution of 4 mM sodium tungstate solved in 50 ml of double distilled water was added. The final suspension was constantly stirred at 60 °C during 1 h leading to precipitation. The precipitate was filtered with a borosilicate filter, washed thoroughly with double bidistilled water, and dried in an oven at 100 °C during 24 h to get the $HgWO_4$ powders.

Structural characterization at ambient pressure was performed by powder XRD measurements at room conditions with the $K_{\alpha 1}:K_{\alpha 2}$ copper radiation in a Rigaku Ultima IV diffractometer. Microanalysis and scanning electron microscopy measurements (not shown) evidence the presence of Hg, W, and O in our powders and an average powder size of 250 nm. High-pressure angle-dispersive x-ray diffraction measurements on $HgWO_4$ up to 16 GPa were carried out in an Xcalibur diffractometer (Oxford Diffraction Ltd.) using

$K_{\alpha 1}:K_{\alpha 2}$ molybdenum radiation. X-ray diffraction patterns were obtained on a 135 mm Atlas charge-coupled-device (CCD) detector placed at 120 mm from the sample, which was irradiated with an x-ray beam collimated to a diameter of 300 μm. High-pressure measurements were performed in a modified Merrill-Bassett diamond-anvil cell (DAC) with diamond anvils of 500 μm culet size and with an angular range $4\theta=50°$. $HgWO_4$ powder was placed in the 150-μm-diameter hole of the stainless-steel gasket preindented to a thickness of 60 μm. Exposure times were typically of 80 min. An exposure on the starting material in a 0.3 mm glass capillary was obtained using the same installation with the sample to CCD distance of 120 mm. The observed intensities were integrated as a function of 2θ in order to give conventional, one-dimensional diffraction profiles. The CRYSALIS software, Version 171.33.48 (Oxford Diffraction Limited) was used for the data collections and the preliminary reduction in the data. The indexing and refinement of the powder patterns were performed using the CHECKCELL, POWDERCELL, and FULLPROF program packages.

Raman-scattering measurements were performed at room temperature with 2 cm^{-1} resolution in a backscattering geometry using the 632.8 nm line of a HeNe laser and a Horiba Jobin-Yvon LabRam HR UV spectrometer in combination with a thermoelectrically cooled multichannel CCD detector. High-pressure Raman measurements on $HgWO_4$ powders up to 25 GPa were performed in a membrane-type DAC using a 20× large working distance objective and laser power of 2 mW. In both x-ray diffraction and Raman-scattering measurements under pressure a mixture of 4:1 methanol:ethanol was used as quasihydrostatic pressure-transmitting medium and ruby chips evenly distributed in the pressure chamber were used to measure the pressure by the ruby fluorescence method.[21]

III. THEORETICAL DETAILS

Total-energy *ab initio* calculations have been performed within the framework of the density-functional theory using the Vienna *ab initio* simulation package (VASP).[22,23] The recently proposed PBEsol (Ref. 24) prescription for the exchange and correlation energy has been used, although for comparison and further check of the method some calculations were also performed within the local-density approximation (LDA).[25] The projector-augmented wave scheme[26,27] was adopted for the pseudopotentials. The set of plane waves extended up to a kinetic-energy cutoff of 530 eV and dense Monkhorst-Pack grids appropriate to each structure were used to perform integrations in the reciprocal space. With these parameters, highly converged total energies (∼1 meV/f.u.) were obtained for each structure. At each selected volume, the structures were fully relaxed to their equilibrium configuration through the calculation of the forces on the atoms[23] and the stress tensor.[28] In the relaxed equilibrium configuration, forces were lower than 0.002 eV/Å and the deviation of the stress tensor from a diagonal hydrostatic form was less than 1 kbar (0.1 GPa). This high level of accuracy was necessary to perform phonon calculations using the supercell method (see, for example, Refs. 29 and 30 for similar studies).
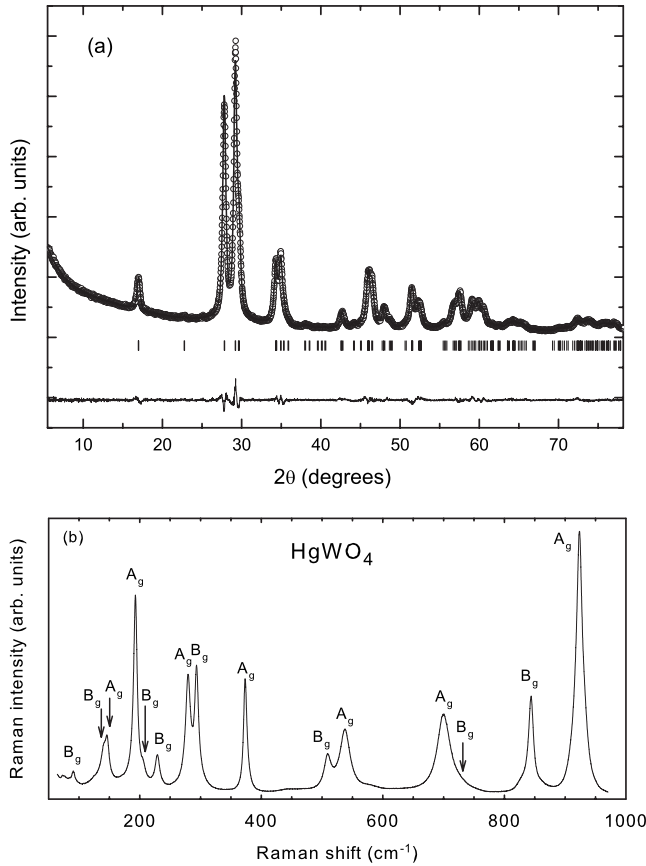
FIG. 2. (a) Diffraction pattern of HgWO$_4$ ($C2/c$, $Z=4$) at room conditions. Open circles: observed intensity, solid lines: calculated and difference XRD profiles. Vertical markers indicate Bragg reflections. (b) Raman-scattering spectrum of HgWO$_4$ at room conditions.

FIG. 3. Room-temperature x-ray diffraction patterns of HgWO$_4$ using the K_α Mo line at different pressures up to 16 GPa.

IV. RESULTS

A. X-ray diffraction measurements under pressure

Figure 2(a) shows the x-ray diffraction pattern of our sample at room pressure using the $K_{\alpha1}:K_{\alpha2}$ cooper radiation. It corresponds to monoclinic ($C2/c$) HgWO$_4$ [inorganic crystal structure database (ICSD) 280305]. A full Rietveld refinement of the XRD pattern obtained at ambient pressure and carried out using the program FULLPROF is also shown in Fig. 2(a). Our refinement yields the unit-cell volume and lattice parameters at room conditions: $V_0=324.04(3)$ Å^3, $a=11.3660(6)$ Å, $b=6.0211(3)$ Å, $c=5.1481(2)$ Å, and $\beta=113.111(1)°$. The fitted standard R_{wp} and R_p factors are 3.7% and 2.8%, respectively, with χ^2 of 1.26. The Bragg residual, R_B is 1.4%. The corresponding R_{wp} and R_p factors without the background are 6.7% and 6.8%, respectively. Table I summarizes the experimental lattice and atomic parameters for the $C2/c$ phase of HgWO$_4$ at room conditions and compares them with those theoretically calculated from first principles using the LDA and PBEsol approximation. Our experimental results compare nicely with those obtained from powders by neutron diffraction and those obtained from single-crystal XRD.[12,13] Our total-energy calculations for the lattice parameters of HgWO$_4$ (see Table I) using the PBEsol
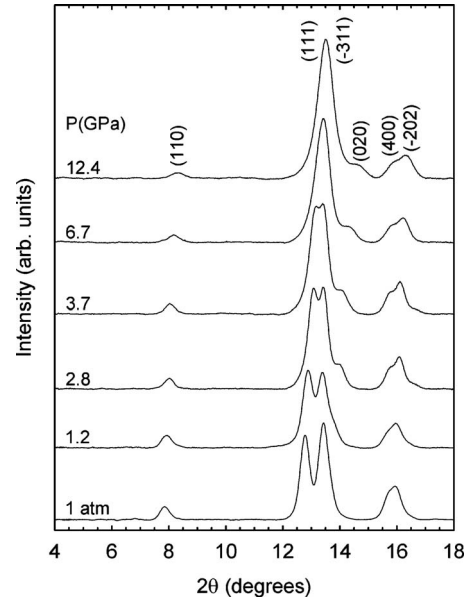
(LDA) approximation are found to agree within 1% (5%) with those obtained from our XRD measurements.

Figure 3 shows the XRD patterns of HgWO$_4$ up to 16 GPa using the $K_{\alpha1}:K_{\alpha2}$ molybdenum radiation. XRD patterns were collected up to 18.9° because of the appearance of the stainless-steel peaks of the gasket at higher angles. Only six peaks of the monoclinic structure can be measured in this angle range. Figure 4 shows the experimental and theoretical pressure dependence of the volume, lattice parameters, and monoclinic β angle of HgWO$_4$ up to 16 GPa. A rather good agreement is found between experiments and calculations. It can be observed that a general better description of the pressure dependence of the structural parameters is obtained for PBEsol calculations than for LDA calculations. A fit of our experimental volume vs pressure data with a third-order Birch-Murnaghan equation of state yields a bulk modulus $B_0=72.7$ GPa and a bulk modulus pressure derivative $B_0'=5.1$ for HgWO$_4$. Our *ab initio* study is in reasonable agreement with the experimental values, giving $B_0=60.6$ (81.4) GPa and $B_0'=8.9$ (7.8) for calculations performed within the PBEsol (LDA) approximation of the exchange and correlation energy.

B. Raman-scattering measurements under pressure

The structure of HgWO$_4$ has 4 f.u. per body-centered unit cell of space group C_{2h}^6 ($C2/c$). Therefore, group theoretical considerations indicate that there should be 36 vibrational modes with the following representation:

$$\Gamma = 7A_g + 10A_u + 8B_g + 11B_u.$$

The 15 gerade (g) modes are Raman active while the 21 ungerade (u) modes are IR active and include the three acoustic modes (A_u+2B_u). In HgWO$_4$, the Hg cation located at a $4c$ Wyckoff site does not contribute with any Raman-active mode in contrast to the β-fergusonite structure of

TABLE I. Experimental and theoretically calculated crystal parameters of monoclinic ($C2/c$, $Z=4$) $HgWO_4$ at room conditions.

	X-ray diffraction[a]	X-ray diffraction[b]	*Ab initio* LDA[a]	*Ab initio* PBEsol[a]
a (Å)	11.3660(6)	11.3791(4)	11.459	11.477
b (Å)	6.0211(3)	6.0079(15)	5.831	6.014
c (Å)	5.1481(2)	5.1456(3)	5.087	5.148
β	113.111(1)°	113.202(3)°	114.625°	113.864°
Hg site: $4c$	$x=0.25$	$x=0.25$	$x=0.25$	$x=0.25$
	$y=0.25$	$y=0.25$	$y=0.25$	$y=0.25$
	$z=0$	$z=0$	$z=0$	$z=0$
W site: $4e$	$x=0$	$x=0$	$x=0$	$x=0$
	$y=0.1887(3)$	$y=0.1868(5)$	$y=0.1914$	$y=0.1880$
	$z=0.25$	$z=0.25$	$z=0.25$	$z=0.25$
O_1 site: $8f$	$x=0.0952(1)$	$x=0.0966(4)$	$x=0.0952$	$x=0.0955$
	$y=0.071(2)$	$y=0.0918(8)$	$y=0.0926$	$y=0.0916$
	$z=0.038(2)$	$z=0.0291(9)$	$z=0.0328$	$z=0.0317$
O_2 site: $8f$	$x=0.1058(1)$	$x=0.1151(5)$	$x=0.1192$	$x=0.1174$
	$y=0.3866(2)$	$y=0.366(1)$	$y=0.3770$	$y=0.3692$
	$z=0.466(2)$	$z=0.472(1)$	$z=0.4845$	$z=0.4796$

[a]This work.
[b]Reference 13.

ABO_4 compounds where the A cation, located at a $4e$ Wyckoff site, contributes with three Raman-active modes. This is the reason why the low-pressure phase of $HgWO_4$ shows only 15 Raman-active modes in contrast to the 18 modes of the β-fergusonite structure of $YNbO_4$ and of $ZnWO_4$ and $CdWO_4$ at high pressures;[15,17] and also in contrast to the 18 modes of the M-fergusonite structure observed in scheelite tungstates at high pressures.[29–32]

Figure 2(b) shows the 15 Raman-active modes of $HgWO_4$ at room conditions. The Raman spectrum is dominated by the stretching mode at 924 cm^{-1}. The frequencies of the measured first-order modes agree with those already reported.[20] Our Raman spectrum at room pressure shows three Raman-active modes below 150 cm^{-1} that were not previously observed. The symmetry of the different Raman modes has been assigned with the help of our *ab initio* lattice dynamics calculations, as can be seen in Table II. It is observed that the frequencies of the measured and calculated Raman-active modes at room pressure agree reasonably well both in the LDA and PBEsol approximations, being the agreement slightly better for the LDA approximation.

Figure 5 shows the Raman spectra of $HgWO_4$ at different pressures up to 25 GPa. Out of the 15 Raman-active first-order modes, we have measured the pressure dependence of 14 modes. Only the weak B_g mode, located at 715 cm^{-1} at room pressure and that appears as a shoulder of an intense and broad Raman peaks in Fig. 2(b), has not been measured under pressure. Figure 6 shows the experimental and calculated pressure dependence of the frequencies of the different Raman-active first-order modes. In general, a good agreement between experimental and calculated frequencies and pressure coefficients can be observed in Table II. The differ-

ence between the LDA and PBEsol calculations is rather small, but the LDA frequencies at room pressure are in slightly better agreement with the experimental values, while the pressure coefficients at room pressure are better reproduced within the PBEsol approximation. For completeness, the calculated frequencies and pressure coefficients of the IR-active modes for $HgWO_4$ are given in Table III together with experimental data at room pressure obtained from Ref. 20.

A curious feature of the Raman spectra of $HgWO_4$ is the almost zero pressure coefficient of the highest-frequency first-order Raman mode and the negative pressure coefficient of the second highest-frequency first-order Raman modes at low pressures below 3 GPa. The pressure coefficient of the highest-frequency mode increases for pressures above 3 GPa. On the other hand, the second highest-frequency Raman mode behaves as a soft mode and decreases monotonically with increasing pressure with a saturation in its decrease above 10 GPa. These behaviors are markedly different to those of the highest-frequency stretching modes of the wolframite and β-fergusonite phases in $ZnWO_4$,[15] and those of the wolframite, triclinic, scheelite, and β-fergusonite phases in $CdWO_4$.[17] Furthermore, they are also markedly different from those of the scheelite and M-fergusonite phases observed in scheelite tungstates at high pressures.[29–32] This behavior will be discussed in the next section. Note that our calculations, plotted as lines in Fig. 6(b), describe rather well the behaviors of these two highest-frequency modes; however, results of LDA calculations show a slightly better agreement with experimental data than those of PBEsol calculations.
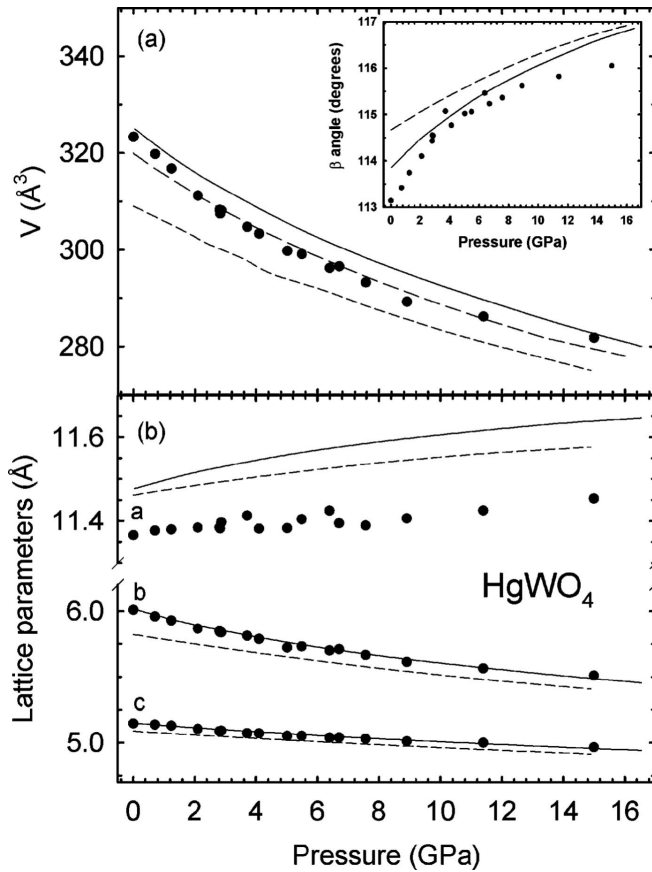
FIG. 4. (a) Pressure dependence of the experimental (symbols) and calculated relative volume of HgWO$_4$ up to 16 GPa. Dashed line shows the fit to a third-order Birch-Murnaghan equation of state. Inset shows the experimental (symbols) pressure dependence of the monoclinic β angle. (b) Pressure dependence of the experimental (symbols) and calculated lattice parameters of HgWO$_4$ up to 16 GPa. In all figures, theoretical data obtained with PBEsol and LDA approximations are noted with solid and short dashed lines, respectively.

V. DISCUSSION

A. Monoclinic HgWO$_4$

Regarding x-ray diffraction results, our experimental bulk modulus of 72.7 GPa and our theoretical ones, 60.6 GPa (81.4 GPa) for PBEsol (LDA) approximation, evidence that HgWO$_4$ is somewhat less compressible than scheelite-type tungstates which feature bulk moduli in the range of 40–70 GPa (Ref. 33) but much more compressible than wolframite-type MgWO$_4$, ZnWO$_4$, and CdWO$_4$ with bulk moduli between 130 and 160 GPa.[16,34] The much smaller bulk moduli of HgWO$_4$ compared to the related wolframites indicates that HgWO$_4$ has a structure less compact than wolframite. The experimental bulk modulus obtained for HgWO$_4$ is in good agreement with the value obtained by the empirical expression proposed in Ref. 14 to estimate the bulk modulus in ABO_4 materials (67 GPa) by considering the average Hg-O bond distance. This agreement suggests that the strong compressibility of HgWO$_4$ is related to the compressibility of HgO$_8$ polyhedra. Figure 7 shows the calculated Hg-O and
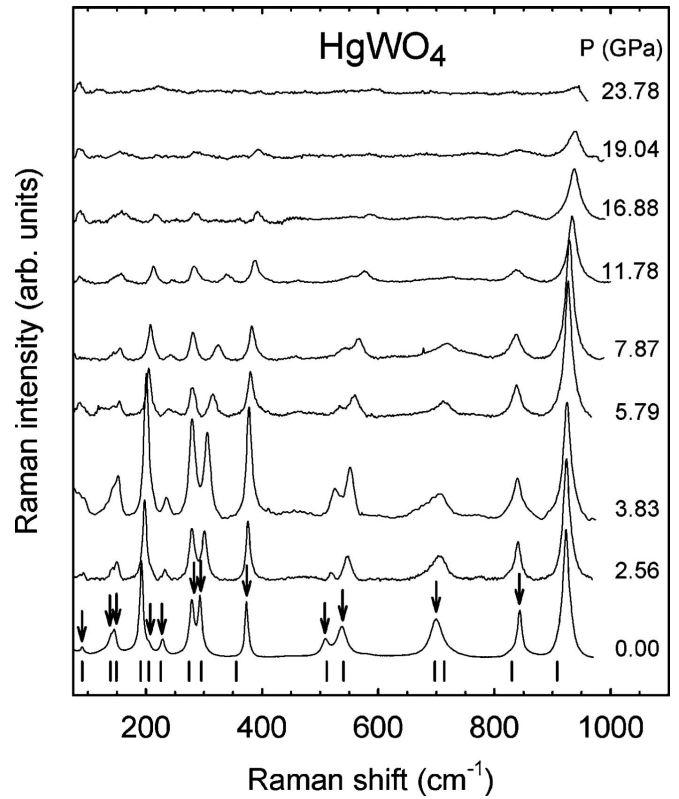

FIG. 5. Raman spectra of HgWO$_4$ at different pressures up to 25 GPa. Arrows and bottom marks indicate the experimental and theoretical (LDA) position of the Raman-active modes at ambient pressure, respectively.

W-O bond distances in HgWO$_4$ as a function of pressure. No experimental data can be shown because we have not been able to perform Rietveld refinements of our x-ray diffraction patterns at different pressures. It can be observed that in fact Hg-O bond distances are more compressible than W-O bond distances and this justifies the use of the empirical formula proposed in Ref. 14 to estimate the bulk modulus of HgWO$_4$. The most notable features of Fig. 7 are the increase in the shortest Hg-O and W-O distances on compression. These behaviors have not been observed in any other tungstate and will be discussed below.

Concerning Raman measurements, the most interesting challenge is to understand the small but positive and the negative pressure coefficients of the two stretching modes of highest frequency. To this end we must remember that the Raman-active modes of AWO$_4$ tungstates can be separated into internal and external modes of the WO$_4$ or WO$_6$ polyhedra.[15,17,29,30] The external modes are characterized by motions of the WO$_4$ or WO$_6$ polyhedra as a whole group with respect to the A countercation. The internal modes are characterized by motions of the O atoms against the W atoms and can be subdivided into stretching modes and bending modes. The short and relatively uncompressible W-O bond distances usually yield internal Raman modes with larger frequencies and smaller pressure coefficients than the external Raman modes. In this context, it is well known that the high-frequency modes above 500 cm^{-1} in AWO$_4$ tungstates are usually the internal stretching modes. Our calculations in

TABLE II. Experimental and calculated Raman-mode frequencies at room pressure and their pressure coefficients in monoclinic $C2/c$ HgWO$_4$ as obtained from fits to the data using equation, $\omega = \omega_0 + (d\omega/dP)P$.

Peak/mode (symmetry)	ω_0 (exp.) (cm^{-1})	$d\omega/dP$ (exp.) (cm^{-1}/GPa)	ω_0 (th.)[a] (cm^{-1})	$d\omega/dP$ (th.)[a] (cm^{-1}/GPa)	ω_0 (th.)[b] (cm^{-1})	$d\omega/dP$ (th.)[b] (cm^{-1}/GPa)
F1 (B$_g$)	89	1.63	87	0.79	91	0.81
F2 (B$_g$)	139	0.50	133	0.24	138	0.15
F3 (A$_g$)	145	1.87	141	0.39	148	0.44
F4 (A$_g$)	193	2.36	184	1.67	192	1.86
F5 (B$_g$)	204	2.38	200	1.35	207	1.26
F6 (B$_g$)	228	2.03	216	1.60	224	1.76
F7 (A$_g$)	278	0.30	268	0.11	270	0.22
F8 (B$_g$)	292	3.73	280	4.84	289	5.04
F9 (A$_g$)	374	1.24	353	1.17	354	0.99
F10 (B$_g$) [c]	508	4.68	491	3.96	509	4.27
F11 (A$_g$) [c]	537	3.99	525	3.15	541	3.53
F12 (A$_g$) [c]	698	2.69	683	2.37	698	2.39
F13 (B$_g$) [c]	715		695	2.37	714	3.50
F14 (B$_g$) [c]	842	−0.93	827	−1.27	823	−1.23
F15 (A$_g$) [c]	924	0.51(0.86)[d]	907	−0.45(0.45)[d]	907	−0.10(0.45)[d]

[a]PBEsol calculations.

[b]LDA calculations.

[c]Stretching modes in the monoclinic $C2/c$ HgWO$_4$.

[d]Values in parenthesis are the linear pressure coefficients above 3 GPa for experimental and LDA data and above 6 GPa for PBEsol data.

fact indicate that the six Raman modes of highest frequency are stretching modes (see marks on Table II) because their eigenvectors show that both Hg and W stay at rest and only O move against W atoms. All other Raman modes of smaller frequencies show eigenvectors in which the Hg atoms are at rest and W and O move. Recently, the assignment of the

internal stretching modes has been obtained in several scheelite[29,30] and wolframite[15,17] orthotungstates after relating the stretching W-O mode frequencies inside the WO$_4$ tetrahedra and WO$_6$ octahedra with the Pauling's bond strengths. Using the approach of Hardcastle and Wachs for HgWO$_4$ it is possible to estimate the formal valence of the W
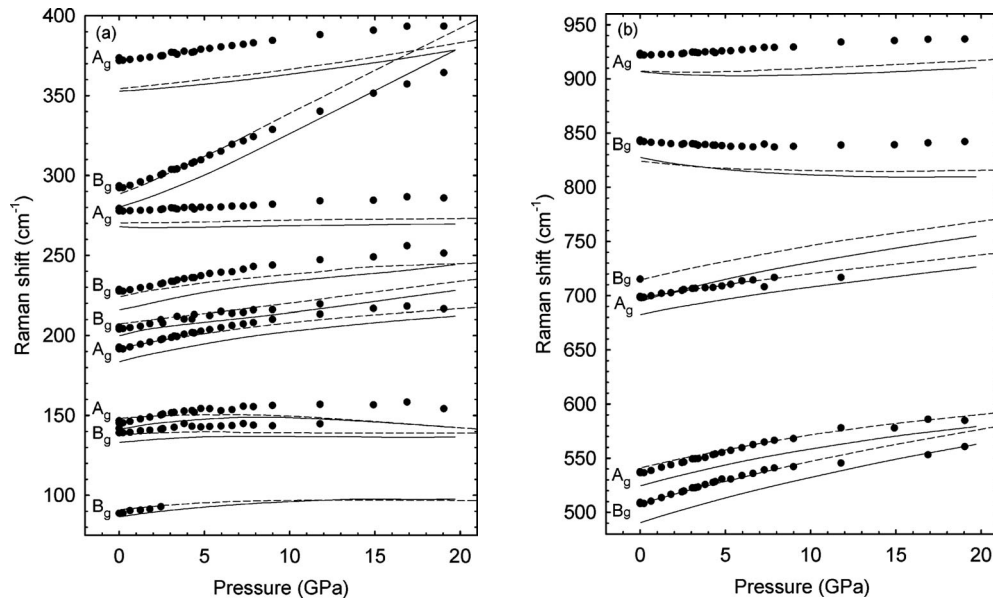

FIG. 6. Pressure dependence of the Raman-mode frequencies of HgWO$_4$ up to 25 GPa. (a) Low-frequency range, (b) high-frequency range corresponding to stretching modes. Symbols correspond to experimental data. Solid lines and short dashed lines correspond to PBEsol and LDA theoretical calculations, respectively.

TABLE III. Calculated infrared-mode frequencies and their pressure coefficients in monoclinic $C2/c$ HgWO$_4$ as obtained from fits to the data using equation $\omega = \omega_0 + (d\omega/dP)P$. Experimental (exp.) data at room pressure are also given for comparison.

Peak/mode (symmetry)	ω_0 [a] (cm^{-1})	$d\omega/dP$ [a] (cm^{-1}/GPa)	ω_0 [b] (cm^{-1})	$d\omega/dP$ [b] (cm^{-1}/GPa)	ω_0 [c] (exp.)
F1 (A$_u$)	0	0	0	0	
F2 (B$_u$)	0	0	0	0	
F3 (B$_u$)	0	0	0	0	
F4 (A$_u$)	52	1.76	58	2.46	
F5 (B$_u$)	60	0.61	67	0.71	
F6 (A$_u$)	71	1.17	75	1.85	
F7 (B$_u$)	78	1.41	84	2.27	
F8 (B$_u$)	138	0.11	145	0.58	
F9 (A$_u$)	140	0.54	146	−0.14	
F10 (B$_u$)	165	1.55	168	2.22	
F11 (A$_u$)	209	3.17	221	3.87	
F12 (B$_u$)	234	−0.44	232	−0.88	250
F13 (B$_u$)	264	1.29	269	0.76	285
F14 (A$_u$)	311	−0.73	308	−1.45	300
F15 (A$_u$)	363	3.90	376	3.87	380
F16 (B$_u$)	469	2.50	484	2.62	490
F17 (A$_u$)	500	1.64	515	1.59	535
F18 (B$_u$)	599	3.13	619	3.33	
F19 (A$_u$)	675	3.38	692	3.54	660
F20 (B$_u$)	842	0.39	842	0.55	880
F21 (A$_u$)	895	0.59	896	0.64	915

[a]PBEsol calculations.
[b]LDA calculations.
[c]Reference 20.

ion in HgWO$_4$ if we consider all the stretching frequencies of the internal modes of the WO$_6$ octahedra. Taking as stretching modes in HgWO$_4$ the six highest-frequency modes at room pressure as suggested by our calculations (see Table II), we obtain a total bond strength of 6.4 v.u. which is in rather good agreement with the valence of 6 for W.

According to Hardcastle and Wachs,[35] the Raman-mode frequency of the stretching modes in tungstates should correlate to the W-O bond lengths. Therefore, the pressure dependence of the frequencies of the two highest-frequency modes should correlate to the pressure dependence of the shortest W-O bond distance. In this respect, the small positive and negative pressure coefficients of the two highest-frequency stretching modes in HgWO$_4$ suggests an increase in the shortest W-O bond distance in good agreement with the calculated increase in the shortest W-O distance plotted in Fig. 7(a). The negative pressure coefficient of the second Raman mode of highest frequency and its saturation above 10 GPa can be understood in the light of theoretical calculations. According to our calculations, there is an increase in the shortest W-O bond length leading to the negative pressure coefficient of this mode. Additionally, there is a saturation of the increase in this bond length above 10 GPa that leads to the decrease in the negative pressure coefficient above 10 GPa which eventually leads to a zero pressure co-

efficient of this Raman mode. The apparent slight increase in the experimental pressure coefficient of this mode above 10 GPa is not confirmed by our calculations and could be due to experimental errors in the estimation of the Raman-mode frequency due to the considerable broadening of this peak above 10 GPa (see Fig. 5).

Regarding the small but positive pressure coefficient of the highest-frequency Raman mode, we can note that several authors consider that the classification of the Raman modes in ABO_4 compounds into internal and external modes of the BO_4 or BO_6 polyhedra is not correct. This classification is used by Hardcastle and Wachs, on the basis of the diatomic approximation, which establishes a direct relationship between the frequency of an internal stretching Raman mode and a given B-O bond length. However, this approximation is not fully consistent provided that the BO_4 or BO_6 polyhedra are considerably distorted, as it is the case in HgWO$_4$.[35–37] Tarte and Liegeois-Duyckaerts already noted strange behaviors of the stretching modes in scheelite-type ABO_4 tungstates and molybdates on changing either A or B cation (A=Ca, Sr, Ba, and Pb, B=Mo and W).[36,37] They considered that the behaviors of the stretching modes could be related to the non-negligible interactions between neighboring BO_4-BO_4 polyhedra. However, our calculations suggest another possibility for the explanation of the strange behav-
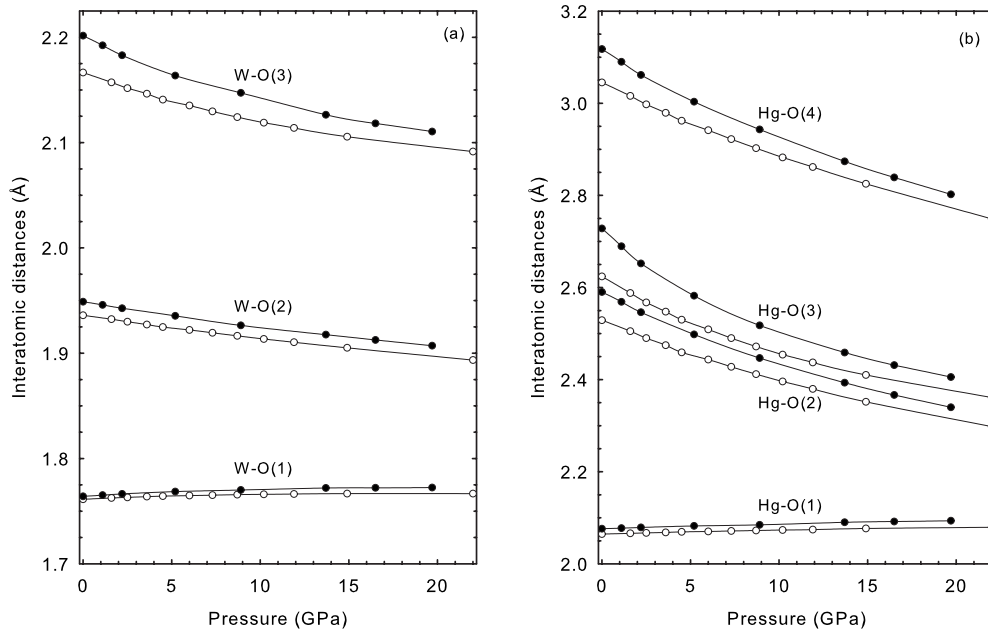
FIG. 7. Calculated pressure dependence of the (a) W-O and (b) Hg-O bond distances in the $C2/c$ structure of HgWO$_4$. Full symbols correspond to PBEsol data while empty symbols correspond to LDA data.

ior observed in the pressure dependence of the two highest-frequency stretching modes of HgWO$_4$ beyond the diatomic approximation. Our calculations indicate that the six O atoms surrounding W in the WO$_6$ octahedra undergo significant displacements in the symmetric stretching A$_g$ mode of highest frequency in HgWO$_4$. In fact, visualization of the theoretical Raman modes with the MOLEKEL program allow us to see that the symmetric stretching A$_g$ mode behaves like a breathing mode with the six O atoms vibrating in phase against the W atom despite the two shortest O2 atoms show larger displacements than the other four O1 atoms. This behavior contrast with the simulation of the asymmetric stretching B$_g$ mode of highest frequency in which basically only the two O2 atoms vibrate out of phase against the W atom with the O1 atoms being almost at rest. These results indicate that the symmetric stretching A$_g$ Raman mode in HgWO$_4$ cannot be assigned to the shortest W-O bond length as in the diatomic approximation but to a larger average W-O bond length due to the contribution of O1 atoms in the vibration. Assuming a small decrease in this average bond length on increasing pressure one could explain the observed small increase in frequency for the symmetric stretching A$_g$ Raman mode in HgWO$_4$ on increasing pressure. Note that the coupled diatomic interactions in the WO$_6$ octahedra would lead to coupling between different Raman modes of equal symmetry, in particular, of A$_g$ symmetry in HgWO$_4$. Therefore, the coupled interactions between W and O atoms in the distorted WO$_6$ octahedra of HgWO$_4$ could be the reason for the positive pressure coefficient of the symmetric stretching A$_g$ modes of highest frequency in HgWO$_4$. Similarly, the uncoupled or slightly coupled stretching B$_g$ modes in HgWO$_4$ allow to explain the soft-mode behavior of the highest-frequency B$_g$ mode in good agreement with the diatomic approximation.

Furthermore, the coupling between stretching A$_g$ modes, that causes a positive positive coefficient for the stretching

A$_g$ mode of highest frequency, would likely lead to a decrease in the pressure coefficient of the other A$_g$-coupled mode due to the contribution of the O2 atoms into the vibration. Indeed, it can be observed in Table II that the pressure coefficient of the second highest-frequency A$_g$ stretching mode is considerably smaller than that of the third one. Therefore, our calculations point to the coupling between the two A$_g$ modes of highest frequency in order to explain the lack of soft-mode behavior for the A$_g$ mode of highest frequency and the smaller pressure coefficient of the second highest A$_g$ mode than the third highest A$_g$ mode.

In order to understand the high-pressure behavior of HgWO$_4$ and its relation to wolframite-type tungstates, we have plotted the three smaller A-O bond distances [Fig. 8(a)] and the three W-O distances [Fig. 8(b)] in several wolframite-type tungstates and HgWO$_4$ at room pressure, as a function of the A cation ionic radius obtained by Shannon.[38] It can be observed that the WO$_6$ octahedra in HgWO$_4$ is composed of two pairs of short W-O bonds of 1.74 and 1.96 Å and another one showing a much larger bond length (2.20 Å). This makes WO$_6$ octahedra in HgWO$_4$ rather distorted in comparison to those in the wolframite structure of ZnWO$_4$ and CdWO$_4$, where all W-O bond distances are more similar. In wolframite ZnWO$_4$ (CdWO$_4$), the W-O distances are 1.79 (1.78), 1.91 (1.92), and 2.13 (2.15) Å. However, on average the W-O distances of the WO$_6$ octahedra in HgWO$_4$ are similar to those in wolframite tungstates.

It can be observed in Fig. 7(a) that, while the longer W-O bond distances decrease under compression as it occurs in wolframite tungstates,[15,17] the shorter W-O bond distance increases with increasing pressure. This increase is responsible for the negative pressure coefficient of the second highest-frequency Raman mode and the small positive pressure coefficient of the highest-frequency Raman mode. Furthermore, it can be observed that the theoretical estimates of the
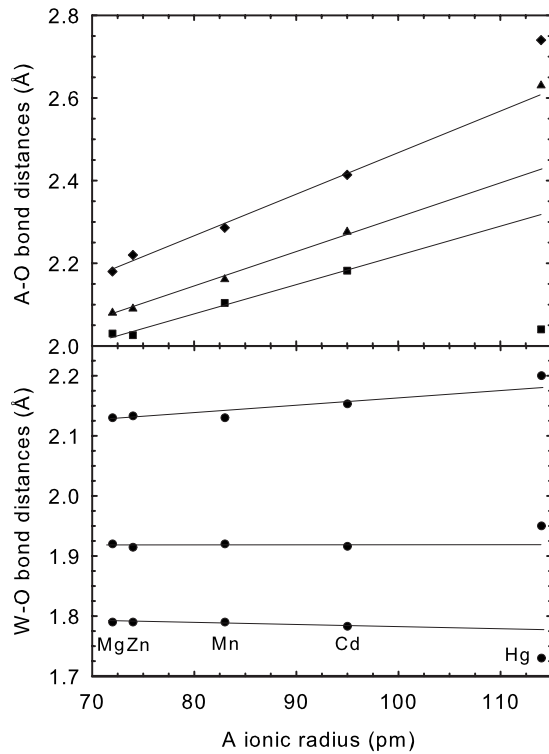
FIG. 8. Experimental A-O and W-O bond distances in wolframite-type AWO$_4$ compounds and in HgWO$_4$ as a function of A ionic radius as obtained from x-ray diffraction data in the literature.

W-O bond distances in HgWO$_4$ at 24 GPa are similar to those observed in wolframite-type CdWO$_4$ at room pressure. Therefore, the rapid decrease in the longest W-O bond distance and the increase in the shortest W-O bond distance with compression evidences that the distorted WO$_6$ polyhedra in the low-pressure phase of HgWO$_4$ tend to become more symmetric on increasing pressure and more similar to those found in wolframite-type tungstates. Therefore, octahedral W coordination is stabilized in HgWO$_4$ at high pressures.

As regards Hg-O bond distances, the HgO$_8$ polyhedra of HgWO$_4$ are very distorted (see Fig. 1). Figure 7(b) shows that the behavior of Hg-O bond distances under compression is similar to that of the W-O bond distances: The smaller Hg-O bond distance increases with compression while the other three longer Hg-O bond distances decrease with increasing pressure. Therefore, our calculations indicate that there is a decrease in the asymmetry of the HgO$_8$ polyhedra in HgWO$_4$ on compression and that eightfold Hg coordination is stabilized in HgWO$_4$ at high pressures. In summary, our total-energy calculations show that HgWO$_4$ is a compound with [6+2,4+2] cation coordination that encompasses [8,6] cation coordination on increasing pressure. Note however, that there is no soft Raman mode associated to the increase in the shorter Hg-O bond distance with pressure. The main reason is that Raman selection rules do not allow Raman modes associated to Hg because the Hg atom is at a 4c Wyckoff site. However, two of the lowest-frequency Raman modes in HgWO$_4$ near 150 cm^{-1} exhibit a very

small pressure dependence and even show a calculated softening above 5 GPa [see Fig. 6(a)]. The behavior of these two modes could be related to the small increase in the shortest Hg-O bond distance with pressure since these low-frequency modes are translational modes related to translation movements of the WO$_6$ octahedra against the Hg atom. A similar decrease in the frequency of the external modes has not been observed previously in wolframite-type related tungstates.[15,17]

Finally, it is worth to compare the A-O bond distances in the different wolframite-type AWO$_4$ compounds related to HgWO$_4$. Figure 8(a) shows the three A-O distances at room pressure in different wolframite-type tungstates compared to those of the three smaller Hg-O distances in HgWO$_4$. In HgWO$_4$, the O-Hg-O angles are 180° in the HgO$_8$ polyhedra in contrast with the 160° value for the O-Zn-O angles of wolframite-type ZnWO$_4$. Additionally, two Hg-O bond lengths are much larger (3.42 Å) than the other six lengths (2.04, 2.63, and 2.73 Å). At room pressure, the Zn-O bond lengths are 2.02, 2.09, and 2.23 Å (average 2.11 Å) in wolframite ZnWO$_4$, and the Cd-O bond lengths are 2.18, 2.27, and 2.41 Å (average 2.29 Å) in wolframite CdWO$_4$. Following the Zn-Cd-Hg sequence of ionic radii one would expect for wolframite HgWO$_4$ the following Hg-O bond lengths: 2.34, 2.45, and 2.59 Å (average 2.46 Å). It can be noted that the two intermediate Hg-O bond lengths in HgWO$_4$ scale with the two largest A-O bond lengths in wolframites when following the Zn-Cd-Hg series in Fig. 8(a). This is a consequence of the larger size of Hg than that of Zn and Cd. However, the shortest Hg-O bond length in HgWO$_4$ does not scale with the shortest A-O bond lengths in the corresponding wolframites. The strong decrease in the shortest Hg-O bond length can only be understood by the tendency of Hg towards eightfold coordination because of its large radius compared to Zn and Cd. In HgWO$_4$ the average Hg-O bond length is 2.71 Å which is larger than the average bond length 2.46 Å expected for wolframite-type HgWO$_4$. The net increase in the Hg-O average bond length in HgWO$_4$ is characteristic of an increase in Hg coordination from 6 to 8.

B. Possible high-pressure phases of HgWO$_4$

We would like to finish our discussion with a hint about the possible high-pressure phases of HgWO$_4$. In our *ab initio* study we have analyzed the relative stability under pressure of different structures: the monoclinic (SG No. 15, $C2/c$, $Z=4$) structure of HgWO$_4$ at room pressure; M-fergusonite (SG No. 15, $I2/a$, $Z=4$); wolframite (SG No. 13, $P2/c$, $Z=2$); scheelite (SG No. 88, $I4_1/a$, $Z=4$); BaZnCl$_4$-type (SG No. 60, $Pbcn$, $Z=4$); SrUO$_4$-type (SG No. 57, $Pbcm$, $Z=4$); CaUO$_4$-type (SG No. 166, R-3m, $Z=1$); BaWO$_4$-II-type (SG No. 14 $P2_1/n$, $Z=8$); and $Cmca$ (SG No. 64, $Cmca$, $Z=8$). On the basis of packing efficiency arguments, as reflected by Bastide's diagram,[18] all these structures are likely high-pressure stable phases of HgWO$_4$, and indeed some have been found to be energetically competitive in previous studies of ABX_4 compounds.[19] Figure 9 shows the energy as a function of volume curves of these structures calculated within the PBEsol approxima-
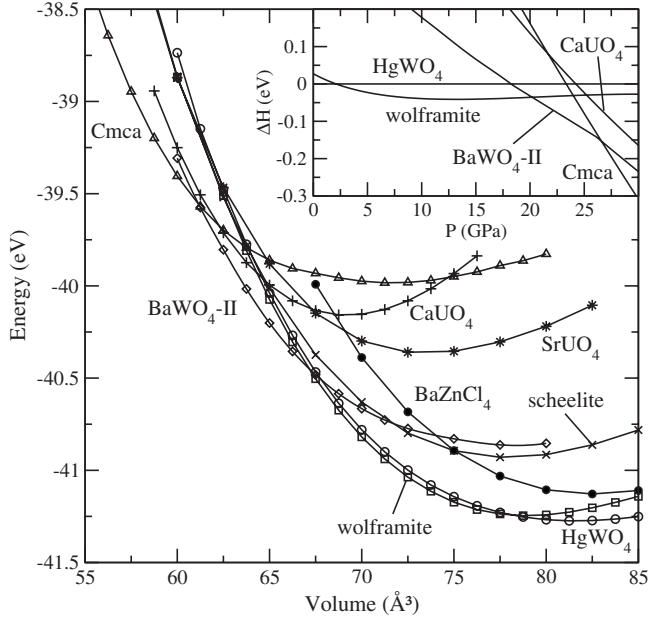
FIG. 9. Total energy as a function of volume plot for the HgWO₄-type (white circles), wolframite (squares), BaZnCl₄-type (black circles), scheelite (crosses), BaWO₄-II-type (diamonds), SrUO₄-type (stars), *Cmca* (triangles), and CaUO₄-type (plus signs) structures. The inset shows the enthalpy as a function of pressure curves of the most stable phases according to our *ab initio* calculations. At each pressure the enthalpy is measured with respect to the enthalpy of the HgWO₄-type structure. Energy, volume, and enthalpy are written per formula unit.

tion for the exchange and correlation energy. The corresponding curves for the LDA calculations show similar energy differences between the different structures and are thus omitted. The M-fergusonite structure was found to be indistinguishable from the scheelite in all the pressure range considered. At ambient pressure, the monoclinic $C2/c$ structure is the most stable among all the ones considered, but it becomes unstable with respect to the wolframite at the rather low pressure of 2 GPa. However the difference in enthalpy between the two structures is rather small, ~40 meV/f.u. both within the PBEsol and LDA approximations, and temperature effects not taken into account in our calculations could reduce it further. This could explain the lack of experimental evidence of a stable wolframite phase at ambient conditions. Regarding the possible phase transition from the $C2/c$ to the wolframite phase, we want to comment that it has not been observed neither by our XRD data nor by our Raman data. If such phase transition would take place between 2 and 5 GPa we should have noted in our XRD spectra the disappearance of the (110) and (310) peaks of the $C2/c$ phase around 8° and 13.7°, and the appearance of the (110) peak of the wolframite phase around 10.6°. Additionally, we should have observed three new Raman modes arising from the change in atomic position of the Hg atom. Therefore, we are confident that no phase transition in this pressure range is observed. Additionally, our calculated pressure dependence of the volume, lattice parameters, and Raman modes in the $C2/c$ phase agree nicely with our measured values, therefore excluding the $C2/c$ to wolframite phase transition.

TABLE IV. Calculated (PBEsol) crystal parameters of the BaWO₄-II phase of HgWO₄ at 20 GPa. Space group $P2_1/n$ with $Z=8$.

$a=11.6941$ Å, $b=6.7145$ Å, $c=6.6287$ Å, $\beta=87.53°$			
Atom	Site	x	y	z
Hg	4e	0.1543	0.6626	0.1536
Hg	4e	0.1352	0.9384	0.6204
W	4e	0.0896	0.1648	0.0889
W	4e	0.1046	0.4596	0.6382
O₁	4e	0.0846	0.0308	0.3225
O₂	4e	0.1996	0.5857	0.8039
O₃	4e	0.0444	0.6606	0.4694
O₄	4e	0.2375	0.2379	0.0729
O₅	4e	0.0785	0.2398	0.8022
O₆	4e	0.1964	0.3500	0.4532
O₇	4e	0.0269	0.4083	0.1656
O₈	4e	0.0856	0.9041	0.9477

Our PBEsol (LDA) calculations show that at pressures above 18.2 (18.6) GPa the fergusonite like $C2/c$ structure is unstable with respect to the BaWO₄-II-type structure. Table IV summarizes the calculated lattice parameters and atomic positions of this structure at 20 GPa. In our Raman measurements up to 25 GPa we have not observed this transition, but it should be noted that calculations yield the thermodynamic equilibrium pressure, which usually is lower than the experimental phase transition pressure, especially in first-order phase transitions like the present one. Experiments at higher pressures or a combination of experiments at different pressures and temperatures should be performed to clarify this point.

Our calculations show that at pressures above 25.5 GPa the BaWO₄-II-type structure becomes unstable with respect to the *Cmca* structure. Full *ab initio* structural data of this phase at 30 GPa is reported in Table V. Our theoretical results show that the complete series of IIB tungstates (AWO_4, $A=$Zn, Cd, and Hg) could undergo a phase transition toward the *Cmca* structure to reach eightfold coordination for W at high pressures. The theoretical pressure at which the phase transition toward the *Cmca* structure is found decreases in

TABLE V. Calculated (PBEsol) crystal parameters of *Cmca* phase of HgWO₄ at 30 GPa. Space group *Cmca* with $Z=8$.

$a=7.0251$ Å, $b=12.8885$ Å, and $c=5.1909$ Å			
Atom	Site	x	y	z
Hg	8e	0.25	0.1796	0.25
W	8f	0	0.4231	0.2323
O₁	8e	0.25	0.3600	0.25
O₂	8f	0	0.1972	0.5001
O₃	8d	0.6614	0	0
O₄	8f	0	0.0785	0.0965

the series, from 58 GPa in $ZnWO_4$,[15] to $\sim$30 GPa in $CdWO_4$,[39] and finally to 26.6 (24.3) GPa in $HgWO_4$, calculated within the PBEsol (LDA) approximation. This decrease in the phase transition pressure in the series is in good agreement with crystal-chemical considerations and is similar to the decrease in the phase transition pressure from the scheelite to the M-fergusonite structure found in scheelite-type AWO_4 (A=Ca, Sr, Pb, and Ba) compounds.[14,19]

VI. CONCLUSIONS

X-ray diffraction and Raman-scattering measurements in the monoclinic $C2/c$ phase of $HgWO_4$ at room conditions have been performed. The 15 Raman-active modes of $HgWO_4$ have been measured and their symmetries have been assigned with the help of lattice dynamics *ab initio* calculations, which have also provided the IR-active modes at room pressure. The Raman spectrum of $HgWO_4$ at room pressure is indicative of the octahedral (4+2) coordination of W in the monoclinic $C2/c$ phase.

X-ray diffraction measurements up to 16 GPa have allowed us to obtain the bulk modulus of $HgWO_4$ and the pressure dependence of its lattice parameters. It is found that $HgWO_4$ is more compressible than wolframite-type tungstates but less compressible than scheelite-type tungstates. On the other hand, our total-energy *ab initio* calculations evidence that the shortest Hg-O and W-O bond distances increase with pressure; a completely different behavior to what is found in related wolframite-type and scheelite-type tungstates. *Ab initio* calculations show that on compression both HgO_8 and WO_6 polyhedra become more symmetrical in the monoclinic $C2/c$ structure and Hg coordination increases from 6+2 to 8 and W coordination increases from 4+2 to 6.

Raman-scattering measurements up to 25 GPa have allowed us to measure the pressure dependence of the frequency of 14 first-order Raman-active modes. The two highest-frequency Raman-active modes show a strange behavior and, in particular, the negative pressure coefficient of the second highest-frequency Raman mode clearly correlates with the increase in the shortest W-O bond length on compression. The pressure dependence of all the Raman-active modes is well described by our lattice dynamical *ab initio* calculations for the monoclinic $C2/c$ phase up to the maximum pressure attained in our experiments.

Finally, a sequence of phase transitions from the monoclinic $C2/c$ phase to the monoclinic $BaWO_4$-II-type and then to the orthorhombic $Cmca$ structure is theoretically predicted with W reaching eightfold coordination in the last structure. Since the $Cmca$ phase is also predicted to be the high-pressure phase of $ZnWO_4$ and $CdWO_4$, this structure is proposed to be a common phase in all wolframite-type tungstates and $HgWO_4$ at high pressures.

*Corresponding author; fjmanjon@fis.upv.es

†On leave from the Indian Institute of Technology of Kharagpur (India).

[1] T. A. Edison, Nature (London) **53**, 470 (1896).

[2] W. Chen, Y. Inagawa, T. Omatsu, M. Tateda, N. Takeuchi, and Y. Usuki, Opt. Commun. **194**, 401 (2001).

[3] P. Lecoq, I. Dafinei, E. Auffray, M. Scheegans, M. V. Korzhik, O. V. Missetvich, V. B. Pavlenko, A. A. Fedorov, A. N. Annenkov, V. L. Kostylev, and V. D. Ligun, Nucl. Instrum. Methods Phys. Res. A **365**, 291 (1995).

[4] M. Ishii and M. Kobayashi, Prog. Cryst. Growth Charact. Mater. **23**, 245 (1991).

[5] N. Klassen, S. Shmurak, B. Red'kin, B. Ille, B. Lebeau, P. Lecoq, and M. Schneegans, Nucl. Instrum. Methods Phys. Res. A **486**, 431 (2002).

[6] M. Bravin, M. Bruckmayer, C. Bucci, S. Cooper, S. Giordano, F. von Feilitzsch, J. Hohne, J. Jochum, V. Jorgens, R. Keeling, H. Kraus, M. Loidl, J. Lush, J. Macallister, J. Marchese, O. Meier, P. Meunier, U. Nagel, T. Nussle, F. Probst, Y. Ramachers, H. Sarsa, J. Schnagl, W. Seidel, I. Sergeyev, M. Sisti, L. Stodolsky, S. Uchaikin, and L. Zerle, Astropart. Phys. **12**, 107 (1999).

[7] G. Blasse and G. P. M. van den Heuvel, J. Lumin. **9**, 74 (1974).

[8] R. Lacomba-Perales, J. Ruiz-Fuertes, D. Errandonea, D. Martínez-García, and A. Segura, EPL **83**, 37002 (2008).

[9] R.-P. Jia, C.-O. Yang, Y.-S. Li, J.-H. Yang, and W. Xia, J. Nanopart. Res. **10**, 215 (2008).

[10] A. W. Sleight, Acta Crystallogr., Sect. B: Struct. Crystallogr. Cryst. Chem. **28**, 2899 (1972).

[11] J. Ruiz-Fuertes, D. Errandonea, A. Segura, F. J. Manjón, Z. Zhu, and C. Y. Tu, High Press. Res. **28**, 565 (2008).

[12] M. B. A. Dahlborg, G. Svensson, and T. Ouvarova, Acta Crystallogr., Sect. C: Cryst. Struct. Commun. **56**, 397 (2000).

[13] M. B. A. Dahlborg and G. Svensson, Acta Crystallogr., Sect. C: Cryst. Struct. Commun. **58**, i35 (2002).

[14] D. Errandonea and F. J. Manjón, Prog. Mater. Sci. **53**, 711 (2008).

[15] D. Errandonea, F. J. Manjón, N. Garro, P. Rodríguez-Hernández, S. Radescu, A. Mujica, A. Muñoz, and C. Y. Tu, Phys. Rev. B **78**, 054116 (2008).

[16] J. Ruiz-Fuertes, S. López-Moreno, D. Errandonea, J. Pellicer-Porres, R. Lacomba-Perales, A. Segura, P. Rodríguez-Hernández, A. Muñoz, A. H. Romero, and J. González, J. Appl. Phys. **107**, 083506 (2010).

[17] R. Lacomba-Perales, D. Errandonea, D. Martínez-García, P. Rodríguez-Hernández, S. Radescu, A. Mújica, A. Muñoz, J. C. Chervin, and A. Polian, Phys. Rev. B **79**, 094105 (2009).

[18] J. P. Bastide, J. Solid State Chem. **71**, 115 (1987).

[19] F. J. Manjón, D. Errandonea, J. López-Solano, P. Rodríguez-

Hernández, S. Radescu, A. Mujica, A. Muñoz, N. Garro, J. Pellicer-Porres, A. Segura, Ch. Ferrer-Roca, R. S. Kumar, O. Tschauner, and G. Aquilanti, Phys. Status Solidi B **244**, 295 (2007).

[20] G. Blasse, J. Inorg. Nucl. Chem. **37**, 97 (1975).

[21] K. Syassen, High Press. Res. **28**, 75 (2008).

[22] G. Kresse and J. Hafner, Phys. Rev. B **47**, 558 (1993).

[23] G. Kresse and J. Furthmüller, Phys. Rev. B **54**, 11169 (1996).

[24] J. P. Perdew, A. Ruzsinsky, G. I. Csonka, O. A. Vydrov, G. E. Scuseria, L. A. Constantin, X. Zhou, and K. Burke, Phys. Rev. Lett. **100**, 136406 (2008).

[25] W. Kohn and L. J. Sham, Phys. Rev. **140**, A1133 (1965).

[26] P. E. Blöchl, Phys. Rev. B **50**, 17953 (1994).

[27] G. Kresse and D. Joubert, Phys. Rev. B **59**, 1758 (1999).

[28] O. H. Nielsen and R. M. Martin, Phys. Rev. Lett. **50**, 697 (1983).

[29] F. J. Manjón, D. Errandonea, N. Garro, J. Pellicer-Porres, P. Rodríguez-Hernández, S. Radescu, J. López-Solano, A. Mujica, and A. Muñoz, Phys. Rev. B **74**, 144111 (2006).

[30] F. J. Manjón, D. Errandonea, N. Garro, J. Pellicer-Porres, P. Rodríguez-Hernández, S. Radescu, J. López-Solano, A. Mujica,

and A. Muñoz, Phys. Rev. B **74**, 144112 (2006).

[31] D. Christofilos, S. Ves, and G. A. Kourouklis, Phys. Status Solidi B **198**, 539 (1996).

[32] D. Christofilos, K. Papagelis, S. Ves, G. A. Kourouklis, and C. Raptis, J. Phys.: Condens. Matter **14**, 12641 (2002).

[33] D. Errandonea, J. Pellicer-Porres, F. J. Manjón, A. Segura, Ch. Ferrer-Roca, R. S. Kumar, O. Tschauner, P. Rodríguez-Hernández, J. López-Solano, S. Radescu, A. Mujica, A. Muñoz, and G. Aquilanti, Phys. Rev. B **73**, 224103 (2006).

[34] J. Macavei and H. Schulz, Z. Kristallogr. **207**, 193 (1993).

[35] F. D. Hardcastle and I. E. Wachs, J. Raman Spectrosc. **26**, 397 (1995).

[36] P. Tarte and M. Liegeois-Duyckaerts, Spectrochim. Acta, Part A **28**, 2029 (1972).

[37] M. Liegeois-Duyckaerts and P. Tarte, Spectrochim. Acta, Part A **28**, 2037 (1972).

[38] R. D. Shannon, Acta Crystallogr., Sect. A: Cryst. Phys., Diffr., Theor. Gen. Crystallogr. **32**, 751 (1976).

[39] A. Muñoz, J. López-Solano, and P. Rodríguez-Hernández (private communication).